$\sqrt{2} \times \sqrt{2}R45°$ reconstruction and electron doping at the SrO-terminated $SrTiO_3$(001) surface

Shohei Ogawa, Koichi Kato, Naoki Nagatsuka, Shohei Ogura, and Katsuyuki Fukutani*
Institute of Industrial Science, the University of Tokyo, 4-6-1 Komaba Meguro-Ku, Tokyo 153-8505, Japan
(Received 23 April 2017; revised manuscript received 12 June 2017; published 8 August 2017)

The atomic and electronic structure of $SrTiO_3$(001) surfaces is investigated by low-energy electron diffraction, Auger electron spectroscopy, atomic force microscopy, ultraviolet photoemission spectroscopy (UPS), and theoretical calculations. While the surface is TiO_2-terminated after annealing at 1225 °C for 72 h, an SrO-terminated surface is realized along with a $\sqrt{2} \times \sqrt{2}R45°$ reconstruction after annealing at 1275 °C for 72 h. The stability of the surface structure revealing a $\sqrt{2} \times \sqrt{2}R45°$ is evaluated by first-principles calculations, which shows that the most stable surface is a periodically SrO-deficient surface. Furthermore, UPS measured on the SrO-terminated $\sqrt{2} \times \sqrt{2}R45°$ surface shows an upward band bending as compared to the TiO_2-terminated surface. Neither in-gap nor metallic states are formed by doping electrons to the $\sqrt{2} \times \sqrt{2}R45°$ surface in contrast to the TiO_2-terminated surface.

DOI: 10.1103/PhysRevB.96.085303

I. INTRODUCTION

$SrTiO_3$ is a typical transition metal oxide with the perovskite structure. There exist two possible formally neutral and stable terminations, SrO and TiO_2, for the most stable (001) surface. Previous experiments for $SrTiO_3$(001) surfaces have mainly been conducted for the samples with dominant TiO_2 termination [1] because of the difficulty of preparing the SrO-terminated surface. A chemical etching with buffered HF can completely remove an SrO layer forming a flat TiO_2-terminated surface [2]. In addition, even the sputter-anneal process forms TiO_2-dominant terminations because Sr is preferentially sputtered compared with Ti [3,4].

Attempts to prepare the SrO-terminated surface were made by cleaving $SrTiO_3$ and molecular beam epitaxy (MBE) of an SrO layer. A recent experimental work, on the other hand, has shown the possibility of preparation of SrO-terminated samples by annealing in air at 1300 °C [5]. A theoretical calculation of the surface free energy also shows that the 1×1 SrO-terminated surface is stable under an adequate oxygen pressure and temperature among the surfaces previously reported [6]. The difference in the surface electronic states due to the termination structures was studied from the theoretical point of view [7,8]. A recent theoretical study, furthermore, predicts that spontaneous metalization occurs on the SrO-terminated surface [8].

For the TiO_2-terminated surface, various superstructures such as 2×1, 2×2, 4×4, $c(4 \times 2)$, 6×2, $\sqrt{5} \times \sqrt{5}$, and $\sqrt{13} \times \sqrt{13}$ have been reported depending on the preparation condition as reviewed in previous papers [9,10]. The correlation between the amount of oxygen deficiencies and the surface reconstructions is particularly examined in detail [11]. As for the SrO-terminated surface, on the other hand, scanning tunneling spectroscopy (STS) was conducted for cleaved $SrTiO_3$ surfaces and MBE-grown surfaces, where the TiO_2- and SrO-terminated domains were distinguished with STS [12,13] and in-gap states were observed due to oxygen vacancies [14]. UPS was observed for MBE-grown surfaces [15]. A mixed termination of TiO_2 and SrO was observed after annealing treatments in a recent atomic force microscopy (AFM) study [16], which might be related to surface reconstructions. Nevertheless, the detailed properties of the SrO-terminated surface are yet to be clarified. The effect of electron doping to the SrO-terminated surface is also not known yet. It is widely known that electron doping to the TiO_2-terminated surface forms in-gap states at 1 eV below the Fermi level and two-dimensional metallic states [17]. Angle-resolved photoemission spectroscopy shows the detail of the metallic band structure such that electrons at the metallic states partially occupy the Ti $3d_{xy}$ band and the doubly degenerate Ti $3d_{xz}$ and $3d_{yz}$ bands [18,19]. Modification of the surface electronic structure is also of importance for the physical properties of thin films grown on $SrTiO_3$.

In the present work, motivated by the study by Bachelet *et al.* [5], we investigated the effects of annealing in air on the termination of $SrTiO_3$ to find that the SrO-terminated surface is formed after annealing at 1275 °C. We also found that the SrO-terminated surface reveals $\sqrt{2} \times \sqrt{2}R45°$, which is likely to be caused by SrO deficiency. UPS showed that the electronic band of the SrO-terminated surface is upward bent compared to the TiO_2-terminated surface. Furthermore, we observed the behavior of excess electrons due to hydrogen adsorption and oxygen vacancies on the $SrTiO_3$ surfaces.

II. EXPERIMENTAL AND THEORETICAL METHODS

The sample used in the present work was *n*-type $SrTiO_3$(001) (0.05 wt. % Nb doped). We conducted two kinds of processes for preparing surfaces with different terminations. One was annealing in the air, and the other was the sputter anneal in an ultrahigh vacuum (UHV) (sample:T). In the former process, the $SrTiO_3$ sample was treated by a 3:1 HCl-HNO_3 solution, which is called the Arkansas method removing Sr from the surface [20], and stored in an electric furnace kept at about 1225–1325 °C for 72 h, which is expected to lead to an SrO-dominated termination following the previous study [5]. After introducing the sample into a UHV chamber, the sample was annealed at 600 °C under an oxygen gas (99.999% purity) of 5×10^{-5} Pa for 30 min. In the sputter-anneal process, the sample was annealed at 650 °C under an oxygen pressure of 6.5×10^{-4} Pa for 30 min following Ar sputtering for 10 min

*fukutani@iis.u-tokyo.ac.jp

with an ion current of 2 μA and an energy of 1 keV. Because of the difference of the sputter yield between Sr and Ti atoms [3], a TiO_2-dominant termination is expected to be formed.

We characterized the surfaces by low-energy electron diffraction (LEED), AFM, and Auger electron spectroscopy (AES) at room temperature. LEED and AES measurements were performed in a UHV chamber at a base pressure of $<1 \times 10^{-8}$ Pa and AFM in the dynamic mode was performed in the air. UPS experiments were conducted in a separate UHV chamber at a base pressure of 1×10^{-8} Pa with the He I source (21.2 eV) at an incidence angle of 45° in normal emission at room temperature. The acquisition time was typically 1000 s for a spectrum. X-ray photoemission spectroscopy (XPS) was also conducted in the same chamber with Al Kα (1486.6 eV) to obtain the information about the core-level states of C 1*s*, O 1*s*, Ti 2*p*, and Sr 3*d*.

The interaction of hydrogen with surfaces was investigated with H_2 gas (99.999% purity). As hydrogen molecules hardly react with $SrTiO_3$ (001) surfaces due to the dissociation barrier [21], the surfaces were exposed to hydrogen atoms at room temperature produced by a tungsten filament heated at 2000 K, which is located 5 cm from the sample. Since the dissociation probability is not accurately known, the amount of exposure is indicated by the mixture of H and H_2 in this paper.

We evaluated the stability of the surface structure by theoretical calculations. The calculations are based on density functional theory (DFT) with the generalized gradient approximation (GGA) of PW91. We used the original version of the PHASE code [22]. The cutoff energies are 25 Ry for the wave functions and 196 Ry for the augmented electron densities. The calculations were performed for five layers with the bottom layer of SrO with 4 k points for Brillouin-zone sampling. Inversion symmetry with respect to the slab center is used to enhance the computational efficiency. The structure consists of a $(2 \times 2 \times 5)$ unit cell with periodic boundary conditions. The atomic positions are relaxed accordingly to be in equilibrium positions.

III. RESULT

Figures 1(a_1), 1(b_1), and 1(c_1) show LEED patterns for the samples annealed at 1225, 1275, and 1325 °C, respectively, in air at a primary electron energy of 70 eV, where Fig. 1(a_1) shows 1×1 and Figs. 1(b_1) and 1(c_1) show a $\sqrt{2} \times \sqrt{2}R45°$ pattern. This superstructure has not clearly been reported to date, although it might be related to $c(2 \times 2)$ suggested in a previous STM study [13]. Sample:T shows 1×1 as shown in Fig. 1(d_1), which is consistent with a previous study [23]. Figures 1(a_2), 1(b_2), 1(c_2) and 1(d_2) show the AFM topographic images for the samples corresponding to Figs. 1(a_1), 1(b_1), 1(c_1), and 1(d_1), respectively. The AFM measurements were conducted for three or more samples with the same annealing processes to confirm that these surface morphologies are essentially reproducible. Figure 1(a_2) shows a step-terrace structure indicating an atomically flat surface with a step height of 3.9 Å corresponding to one unit cell of $SrTiO_3$ as clearly shown in the line scan of Fig. 1(a_3). Figure 1(b_2) shows a surface with wide and narrow terraces. Whereas the step height corresponding to a narrow terrace is one unit cell, higher steps are formed for wider terraces. The maximum step height is five unit cells in Fig. 1(b_3). On the other hand, small embedded clusters or precipitates are seen in Fig. 1(c_2). The height of the precipitates is 4–16 Å. The surface morphology with precipitates was reported previously upon annealing the sample at a temperature higher than 1300 °C in a vacuum [24], and the precipitates were identified as SrO_{1-x}. The precipitates in Fig. 1(c_2) are therefore likely to be SrO_{1-x}. Figure 1(d_2) shows narrower terraces of 100–200 nm with a step height of lower than two unit cells. It is reported that the TiO_2-terminated terrace edges meander along [010] and [001], whereas the SrO-terminated terrace edges are curved with a radius of 70–300 nm [25]. In the present study, the sample annealed at 1275 °C showed curved terrace edges, while those of sample:T meandered along [011] and [01$\bar{1}$] (not shown), which are in agreement with the later discussion.

The first derivative AES spectra taken for the samples annealed at 1225, 1275, and 1325 °C are shown in Fig. 2. The intensities are normalized to the peak-to-peak values for the Ti LMM Auger transition at 382 eV. The spectra at 86 and 106 eV in Fig. 2 correspond to the Sr LMM Auger transitions. The Sr AES intensities are clearly different between the three samples. The peak-to-peak values of the Auger peak at 106 eV for Sr and at 382 eV for Ti can be used to evaluate the ratio of Sr to Ti at the surface, because the shape of the peak is unchanged for various surface preparations [24]. The ratios are 1.07, 1.71, and 2.23 for the samples annealed at 1225, 1275, and 1325 °C, respectively.

In order to analyze the termination ratio from these values, we simulated the AES intensity ratio of Sr to Ti with a theoretical formula [26] for the surfaces with various termination ratios on the assumption that TiO_2 and SrO layers are stacked alternately. The calculated values are 1.18 for the 100% TiO_2-terminated surface and 1.86 for the 100% SrO-terminated surface. The surface with a mixed termination is expected to show an intermediate value. On the basis of the calculations, it is considered that TiO_2-dominant and SrO-dominant surfaces are realized for the sample annealed at 1225 and 1275 °C, respectively. The value for the sample annealed at 1325 °C is significantly larger than that expected for the SrO-terminated surface. This is probably due to the precipitates of SrO_{1-x} on the surface, which enhance the Auger signal of Sr compared to Ti. The AES ratio of Sr to Ti for sample:T is 1.27, which indicates 85% TiO_2 termination. On the basis of the LEED, AFM, and AES results, the $SrTiO_3$(001) surface reveals $\sqrt{2} \times \sqrt{2}R45°$ with dominant SrO termination after annealing at 1275 °C for 72 h in the air. Hereafter, this sample is called sample:S.

Previous papers have reported that the $SrTiO_3$ surface shows a reconstruction of the Ruddlesden-Popper (RP) phases as a structure of $Sr_{n+1}Ti_nO_{3n+1}$ [27] and Sr oxide islands [28]. As shown in Fig. 1(b_2), however, no islands are found on the surface, and the observed step heights are the integral multiple of the unit cell, which excludes the possibility of the RP phases for the $\sqrt{2} \times \sqrt{2}R45°$ structure. If the RP phases were realized, the step heights of 1.5 or 3 unit cells would be found [29]. On these bases, we conclude that sample:S is SrO terminated with $\sqrt{2} \times \sqrt{2}R45°$ surface reconstruction.

Figure 3 shows the UPS spectra taken for sample:S and sample:T. The peaks at 5 and 7 eV originate from the π and σ orbitals of the O 2*p* band, respectively. The positions of the

valence band top estimated from these spectra are 2.80 eV for sample:S and 3.11 eV for sample:T below the Fermi level. Assuming that the band gap is 3.17 eV, which is the same as that for the bulk, the conduction band bottom is located at 0.37 eV for sample:S and 0.07 eV for sample:T above the Fermi level. The inset in Fig. 3 shows the spectra around the Fermi level. For sample:T, the spectrum reveals a parabolic shape without any electronic states in the band gap. For sample:S, no specific feature is observed around the Fermi level except for a hump at 2 eV, which is ascribed to the emission due to the 23.1 eV line of He I [4]. Spontaneous metallization, which was predicted theoretically [8], is not observed for this surface. The work function derived from the cutoff of secondary electrons for both samples is about 3.8 eV for the both samples. The XPS spectra of O 1*s*, Sr 3*d*, and Ti 2*p* show no specific difference in the spectral shape between the two samples. A feature is observed at 10 eV in Fig. 3 for sample:S, which probably originates from slight contamination of the surface, because a slight C signal is observed in AES and XPS [18].

Figure 4(a) shows the UPS spectra around the Fermi level before and after exposure of the sample:S surface to 100 and 1000 Langmuir (1 Langmuir $= 1.33 \times 10^{-4}$ Pa s) of H + H_2. The valence band top is gradually shifted downward with increasing H + H_2 exposure, which is found to saturate at 2.99 eV after about 1000 Langmuirs. The work function is also decreased by about 0.2 eV. These results indicate that electron transfer to the surface is induced by hydrogen atom adsorption. Figure 4(a) indicates that no in-gap state is present after adsorption of hydrogen atoms. It is noted that the conduction band minimum estimated from the valence band maximum on the assumption of the band gap of 3.17 eV is located above the Fermi level. Figure 4(b) shows the UPS spectra of sample:T after exposure to H + H_2. An in-gap state is clearly observed as reported in previous studies [21,30].

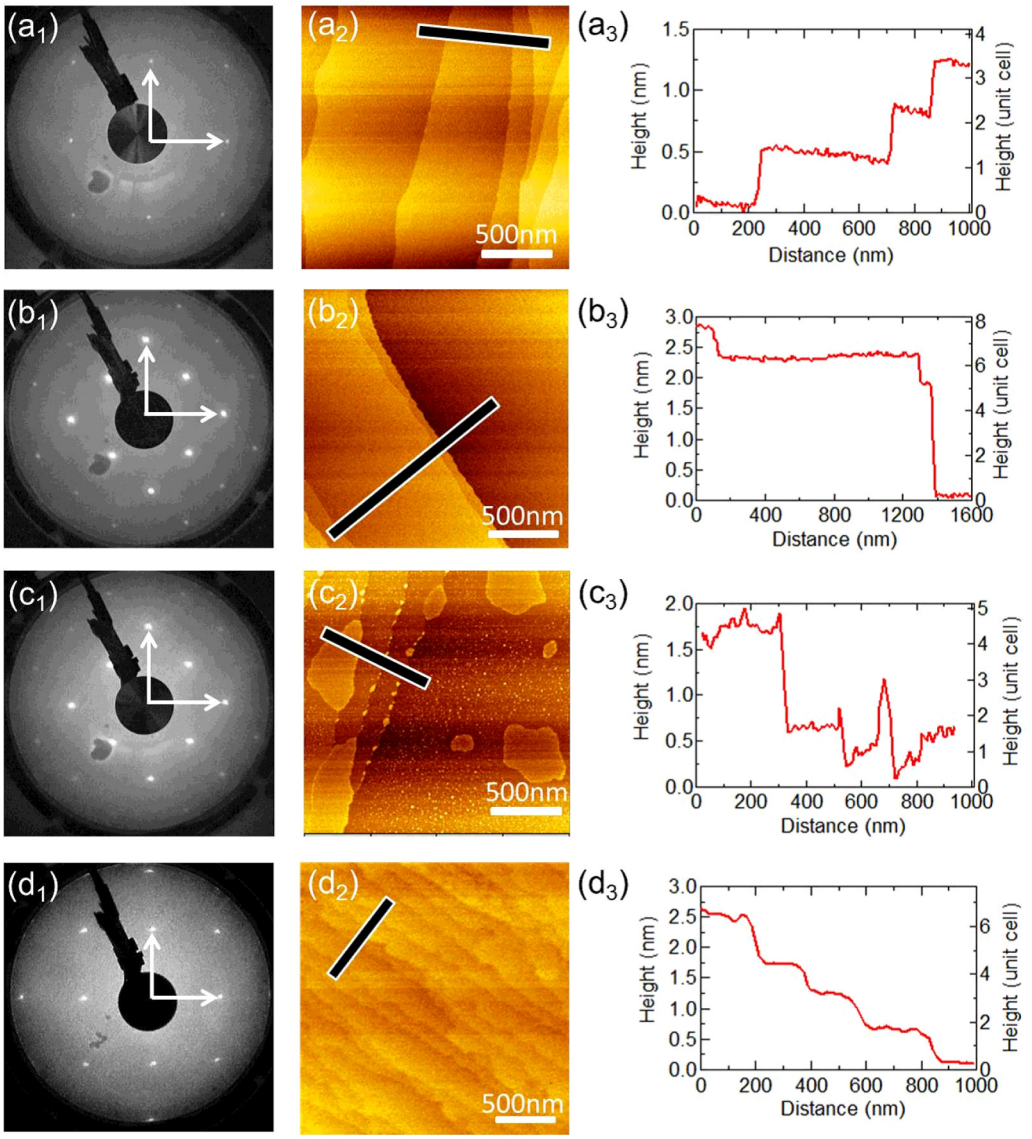

FIG. 1. LEED patterns and AFM images for the $SrTiO_3$(001) surface annealed in air for 72 h at (a) 1225 °C, (b) 1275 °C, and (c) 1325 °C, and (d) sputter annealed. LEED patterns were measured at a primary electron energy of 70 eV. Panels (a_3)–(d_3) show the cross sections along the black lines in (a_2)–(d_2).

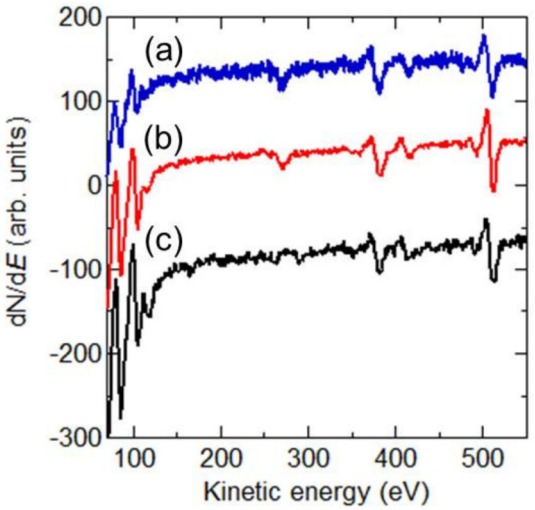

FIG. 2. First derivative Auger spectra corresponding to the Sr LMM, Ti LMM, and O KLL Auger transitions taken for $SrTiO_3(001)$ after annealing at (a) 1225, (b) 1275, and (c) 1325 °C. The intensities are normalized to the peak-to-peak values for the Ti LMM Auger transitions at 382 eV. The peaks at 268 eV correspond to the C KLL Auger transition resulting from slight contamination.

IV. DISCUSSION

It is found that sample:S reveals a $\sqrt{2} \times \sqrt{2}R45°$ structure, and its surface is considered to be SrO terminated. To clarify the atomic structure of this SrO-terminated $\sqrt{2} \times \sqrt{2}R45°$, we evaluate the stability of possible surface structures by DFT calculations. Figures 5(a), 5(b) and 5(c) show three structural models corresponding to $\sqrt{2} \times \sqrt{2}R45°$ assuming that the surface reconstruction is formed by periodic vacancies of O, Sr, and SrO. When Sr and SrO atoms are removed from the surface, the distance between the second layer Ti atom and the third layer O atom is largely elongated. This is presumably due to insufficient charge transfer to the O atoms. The calculated formation energies for the O, Sr, and SrO vacancies are 6.8, 8.1, and 4.9 eV, respectively. Assuming that the frequency factor is a typical value of 10^{15} s^{-1}, the reaction rates for the formation of O, Sr, and SrO at 1275 °C estimated from the formation energies are 7×10^{-8}, 4×10^{-12}, and 1×10^{-1} s^{-1}, respectively. These results suggest that only the SrO-deficient surface is realized during the annealing at 1275 °C for 72 h.

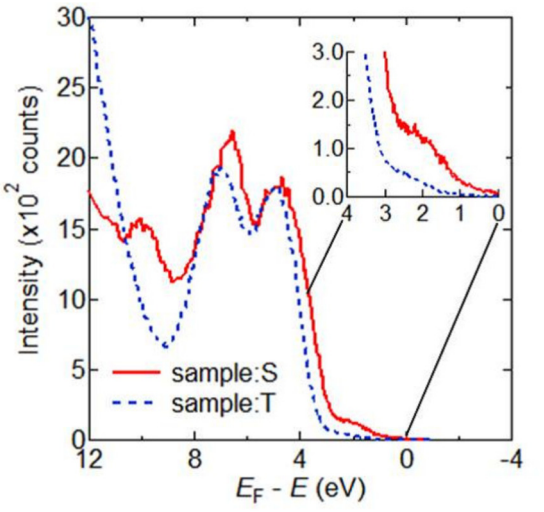

FIG. 3. UPS for sample:S and sample:T taken at room temperature with a photon energy of 21.2 eV.

It is noted that annealing at 1225 °C for 72 h does not lead to the surface reconstruction. The reaction rate forming SrO vacancies at 1225 °C is estimated to be 3×10^{-2} s^{-1}, which is smaller by one order of magnitude than that at 1275 °C. Considering the fact that annealing at 1275 °C for 12 h does not form the surface reconstruction, the difference of the reaction rate by one order of magnitude between 1225 °C and 1275 °C is significant although the reaction rate at 1225 °C derived from the assumed value of the frequency factor seems sufficiently fast to cause the reaction. The selective termination, TiO_2 terminated at 1225 °C and SrO terminated at 1275 °C, is considered to be caused by thermally induced exdiffusion of Sr from bulk [5]. Considering the fact that the surface is initially TiO_2 terminated and that annealing at 1225 °C for 72 h leads to a TiO_2-terminated surface, the exdiffusion of Sr is not sufficiently fast to form an SrO-terminated surface at this temperature.

Whereas sample:S is SrO terminated, sample:T is terminated by the TiO_2 layer. As shown in Fig. 3, the shape of the O 2*p* band is slightly different between the two surfaces. From the fit curves, the peak of the σ orbital at 7 eV for sample:T is found to be broader than that for sample:S. The full width at half maximum for the σ peak is 1.25 eV for sample:T and 1.14 eV for sample:S. This can be explained by the difference in the coordination symmetry of the oxygen atoms around the Ti atom at the outermost surfaces. For the perovskite oxide, the hybridized orbitals of Ti 3*d* and O 2*p* split into doubly degenerate σ orbital and triply degenerate π orbital due to the ligand field. The TiO_6 symmetry is broken into the TiO_5 coordination at the TiO_2-terminated surface, which causes splitting of the originally degenerate states of the σ and π orbitals. The O 2*p* band is expected to be broadened at the TiO_2-terminated surface compared with that on the SrO-terminated surface, because the ligand state is a mixture of TiO_5 and TiO_6 coordination on the TiO_2-terminated surface. The lifting of degeneracy broadens the corresponding band. This is also the reason why the σ peak for sample:T is broadened compared to sample:S. A similar argument is given in previous papers in terms of a theoretical calculation and an experiment for SrO-terminated and TiO_2-terminated surfaces [15,31].

We next discuss the difference around the Fermi level between the two terminated structures after H adsorption. When charges are doped to the $SrTiO_3$ surface, band bending is induced near the surface as demonstrated with oxygen vacancy formation and application of bias voltage [16,23]. It has been shown that the TiO_2-terminated $SrTiO_3$ surface becomes metallic by electron doping through oxygen vacancy formation [19,32] or H adsorption [21,30]. As is expected, the conduction band bottom is considered to be located below E_F forming a metallic state after H adsorption for sample:T. For sample:S, on the other hand, the conduction band minimum is above E_F even after H adsorption without forming metallic

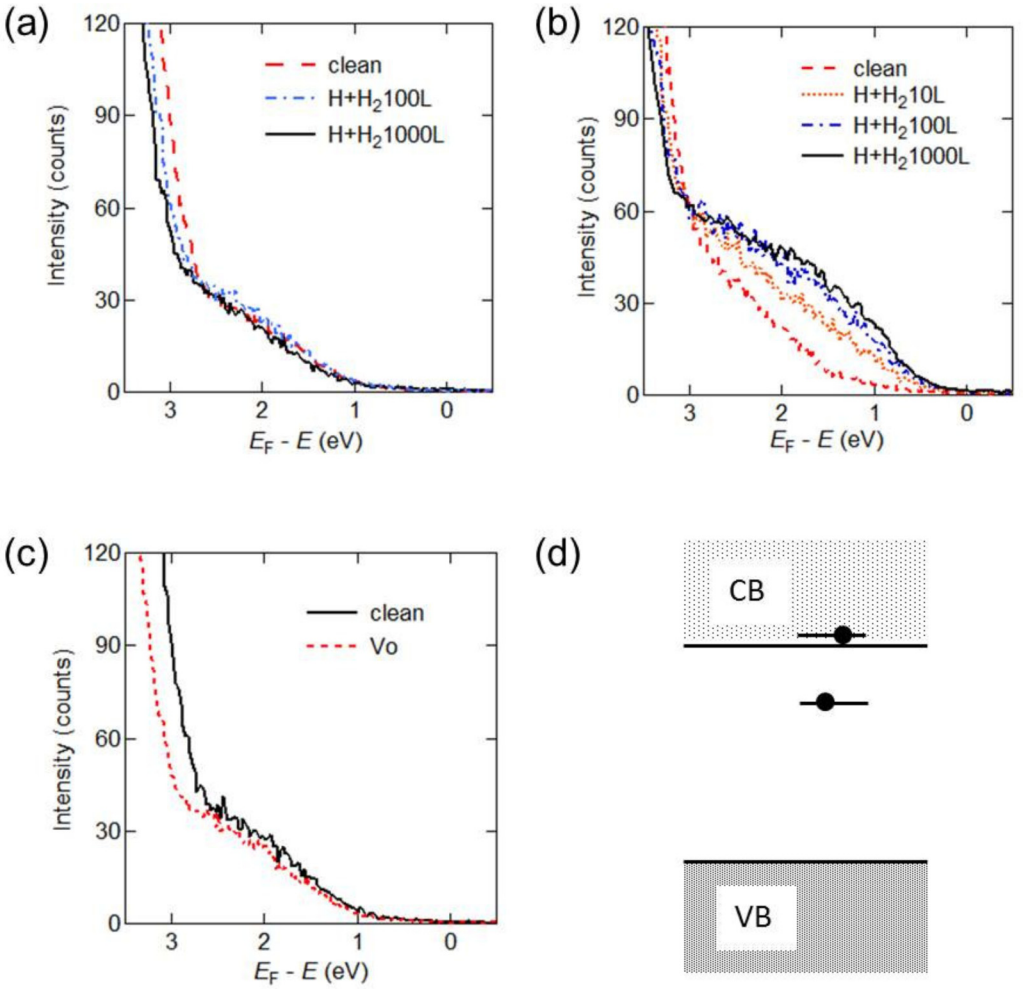

FIG. 4. UPS taken at room temperature with a photon energy of 21.2 eV for (a) sample:S and (b) sample:T before and after exposing the surfaces to $H + H_2$, and (c) sample:S for clean and oxygen-deficient surfaces. (d) Schematic energy level diagram for electron doping in $SrTiO_3$, where polaronic stabilization forms an in-gap state followed by formation of metallic states.

states. This is because the surface band of sample:S is upward bent for some reason such as the surface reconstruction or hole doping.

A previous theoretical study has predicted that the SrO-terminated surface spontaneously becomes metallic [8]. The work shows that a surface potential is formed by electric dipoles resulting from layer-by-layer rumpling, which traps electrons near the surface. Previous experimental work with LEED [33] and RHEED [15] actually reported that the outermost oxygen atoms at the surface are displaced outward by 0.1 Å, which is consistent with *ab initio* calculations [6–8]. On the other hand, sample:S reveals an upward band bending as compared to sample:T. This suggests that the $\sqrt{2} \times \sqrt{2}R45^\circ$ structure forms a surface potential which repels electrons away from the surface.

We discuss the possibility of hole doping with the surface due to O adsorption on the SrO-terminated $\sqrt{2} \times \sqrt{2}R45^\circ$ surface. The present DFT calculations show that the SrO-deficient surface is most likely to appear at the SrO-terminated surface forming $\sqrt{2} \times \sqrt{2}R45^\circ$. However, a small amount of oxygen atoms might adsorb at the O-vacancy sites during annealing in oxygen, which leads to a partially Sr-deficient surface. When Sr is deficient, the surface is doped with holes, which causes an upward band bending at the surface.

Another significant difference between the two terminated surfaces when doped with electrons is formation of an in-gap state. The in-gap state as well as the metallic state was observed when electrons are doped with the TiO_2-terminated surface [17,30]. The in-gap state originates from spatially localized electrons, which are likely to be due to polaron formation. In order to further confirm the effect of electron doping, electron doping is conducted by forming oxygen vacancies. Oxygen vacancies are introduced by vacuum annealing at 400 °C for 15 min, which is reported to be effective for oxygen vacancy formation [34]. From the UPS spectra as shown in Fig. 4(c), downward band bending is observed by 0.2 eV for the oxygen-deficient surface, which is similar to the hydrogen-adsorbed surface. This indicates that the amount of electrons doped to the surface by vacuum annealing is almost the same as the hydrogen-adsorbed surface. It is worth emphasizing that no in-gap state is formed by oxygen vacancy formation.

The in-gap state has been observed in UPS on the TiO_2-terminated surface with electron doping by surface defects including oxygen vacancies and hydrogen adsorption. Since

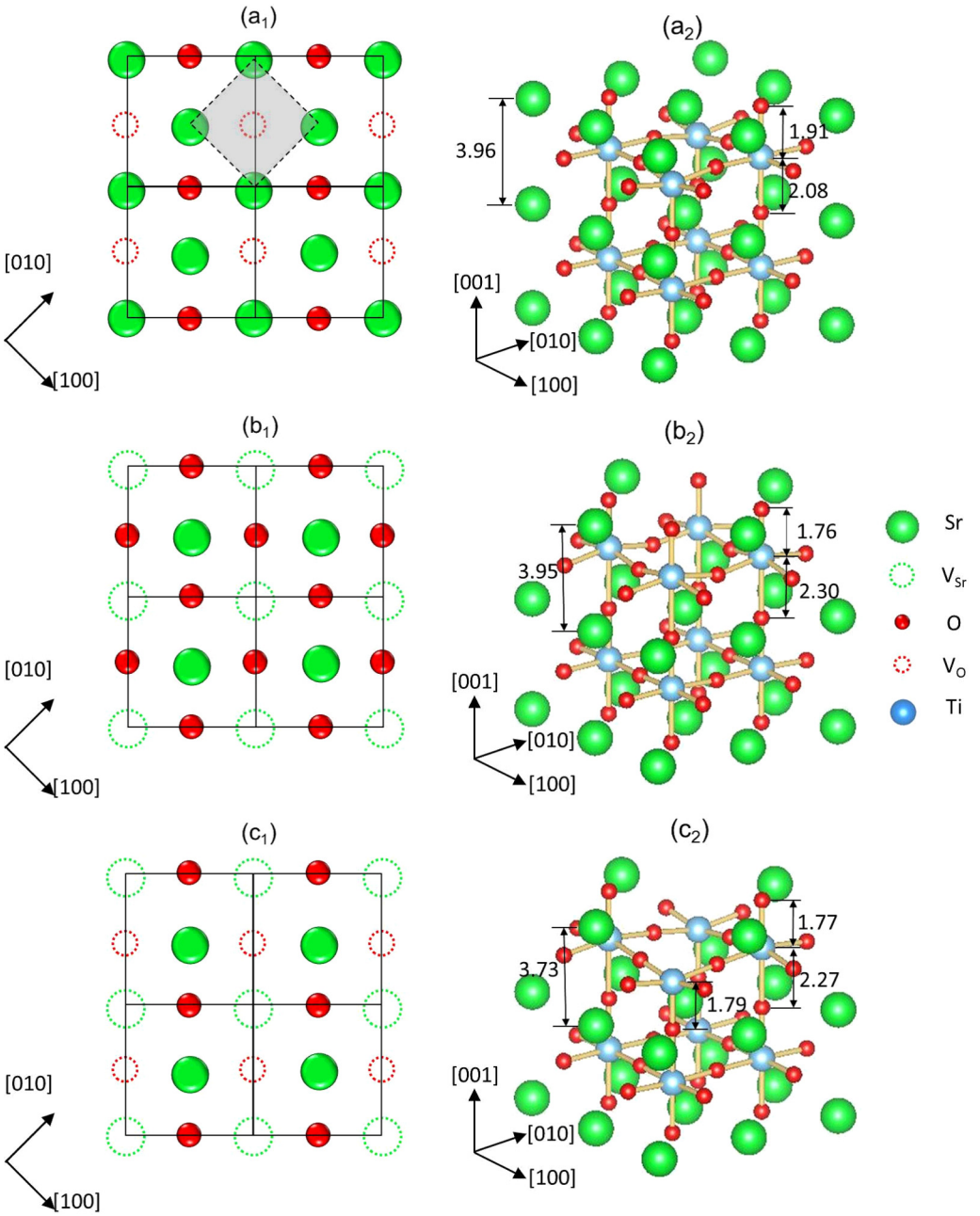

FIG. 5. Structure models corresponding to $\sqrt{2} \times \sqrt{2}R45^\circ$. (a) O-, (b) Sr-, and (c) SrO-deficient surfaces. The amount of the relaxation in the optimized structure is shown in the unit of Å.

the defects might intrinsically be responsible for the in-gap state, the effects of electron doping on the in-gap state formation has not been separated from the effects of surface defects. The present results, on the other hand, obviously show no in-gap state is formed by surface defects of oxygen vacancies and adsorbed H. It is considered that doped electrons diffuse into the bulk due to the upward band bending. This unambiguously indicates that the in-gap state originates from electron doping to the Ti orbital. It is likely that electron doping undergoes polaronic stabilization forming an in-gap state followed by formation of metallic states as shown in Fig. 4(d) [35,36].

In conclusion, we investigated the $SrTiO_3(001)$ surface with LEED, AES, AFM, UPS, and DFT calculations. After annealing the sample at 1275 °C for 72 h, the surface revealed a $\sqrt{2} \times \sqrt{2}R45^\circ$ reconstruction. With the aid of DFT calculations, the reconstructed surface was found to be regularly SrO deficient from the SrO-terminated surface. The electronic states of this reconstructed surface showed upward band bending as compared with the TiO_2-terminated surface. Upon electron doping by H adsorption and oxygen vacancy formation, the SrO-terminated $\sqrt{2} \times \sqrt{2}R45^\circ$ surface exhibited no in-gap states in contrast to the TiO_2-terminated surface that reveals in-gap states along with metallic states.

ACKNOWLEDGMENTS

We thank Professor S. Ashihara and Professor T. Takahashi in our institute for their experimental support for the sample preparation and AFM measurements. This research was supported by JSPS KAKENHI (Grants No. 24246013, No. 26108705, and No. 17H01057).

[1] Y. Aiura, Y. Nishihara, Y. Haruyama, T. Komeda, S. Kodaira, Y. Sakisaka, T. Maruyama, and H. Kato, Physica B (Amsterdam) **194**, 1215 (1994).
[2] M. Kawasaki, T. Maeda, R. Tsuchiya, and H. Koinuma, Science **266**, 1 (1993).
[3] J. E. Mahan and A. Vantomme, Phys. Rev. B **61**, 8516 (2000).
[4] V. E. Henrich, G. Dresselhaus, and H. J. Zeiger, Phys. Rev. B **17**, 4908 (1978).
[5] R. Bachelet, F. Sánchez, F. J. Palomares, C. Ocal, and J. Fontcuberta, Appl. Phys. Lett. **95**, 141915 (2009).
[6] K. Johnston, M. R. Castell, A. T. Paxton, and M. W. Finnis, Phys. Rev. B **70**, 085415 (2004).
[7] E. Heifets, S. Piskunov, E. A. Kotomin, Y. F. Zhukovskii, and D. E. Ellis, Phys. Rev. B **75**, 115417 (2007).
[8] P. Delugas, V. Fiorentini, A. Mattoni, and A. Filippetti, Phys. Rev. B **91**, 115315 (2015).
[9] N. Erdman and L. D. Marks, Surf. Sci. **526**, 107 (2003).
[10] D. S. Deak, Mater. Sci. Technol. **23**, 127 (2007).
[11] R. Shimizu, K. Iwaya, T. Ohsawa, S. Shiraki, T. Hasegawa, T. Hashizume, and T. Hitosugi, Appl. Phys. Lett. **100**, 263106 (2012).
[12] N. P. Guisinger, T. S. Santos, J. R. Guest, T.-Y. Chien, A. Bhattacharya, J. W. Freeland, and M. Bode, ACS Nano **3**, 4132 (2009).
[13] K. Iwaya, R. Shimizu, T. Ohsawa, T. Hashizume, and T. Hitosugi, Phys. Rev. B **83**, 125117 (2011).
[14] W. Sitaputra, N. Sivadas, M. Skowronski, D. Xiao, and R. M. Feenstra, Phys. Rev. B **91**, 205408 (2015).
[15] T. Hikita, T. Hanada, M. Kudo, and M. Kawai, Surf. Sci. **287-288**, 377 (1993).
[16] O. E. Dagdeviren, G. H. Simon, K. Zou, F. J. Walker, C. Ahn, E. I. Altman, and U. D. Schwarz, Phys. Rev. B **93**, 195303 (2016).
[17] Y. Aiura, I. Hase, H. Bando, T. Yasue, T. Saitoh, and D. S. Dessau, Surf. Sci. **515**, 61 (2002).
[18] R. Yukawa, S. Yamamoto, K. Ozawa, M. DAngelo, M. Ogawa, M. G. Silly, F. Sirotti, and I. Matsuda, Phys. Rev. B **87**, 115314 (2013).
[19] A. F. Santander-Syro, O. Copie, T. Kondo, F. Fortuna, S. Pailhès, R. Weht, X. G. Qiu, F. Bertran, A. Nicolaou, A. Taleb-Ibrahimi, P. Le Fèvre, G. Herranz, M. Bibes, N. Reyren, Y. Apertet, P. Lecoeur, A. Barthélémy, and M. J. Rozenberg, Nature (London) **469**, 189 (2011).
[20] M. Kareev, S. Prosandeev, J. Liu, C. Gan, A. Kareev, J. W. Freeland, M. Xiao, and J. Chakhalian, Appl. Phys. Lett. **93**, 061909 (2008).
[21] K. Takeyasu, K. Fukada, S. Ogura, M. Matsumoto, and K. Fukutani, J. Chem. Phys. **140**, 084703 (2014).
[22] PHASE, Institute of Industrial Science, University of Tokyo, http://www.ciss.iis.u-tokyo.ac.jp/english/.
[23] K. Takeyasu, K. Fukada, M. Matsumoto, and K. Fukutani, J. Phys.: Condens. Matter **25**, 162202 (2013).
[24] Y. Liang and D. A. Bonnell, Surf. Sci. **310**, 128 (1994).
[25] J. Fompeyrine, R. Berger, H. P. Lang, J. Perret, E. Machler, C. Gerber, and J.-P. Locquet, Appl. Phys. Lett. **72**, 1697 (1998).
[26] A. Jablonski and C. J. Powell, Surf. Interface Anal. **20**, 771 (1993).
[27] K. H. Lee, S. W. Kim, H. Ohta, and K. Koumoto, J. Appl. Phys. **100**, 063717 (2006).
[28] Y. Liang and D. Bonnell, J. Am. Ceram. Soc. **78**, 2633 (1995).
[29] K. Szot and W. Speier, Phys. Rev. B **60**, 5909 (1999).
[30] M. DAngelo, R. Yukawa, K. Ozawa, S. Yamamoto, T. Hirahara, S. Hasegawa, M. G. Silly, F. Sirotti, and I. Matsuda, Phys. Rev. Lett. **108**, 116802 (2012).
[31] M. Tsukada, C. Satoko, and H. Adachi, J. Phys. Soc. Jpn. **48**, 200 (1980).
[32] P. D. C. King, S. McKeown Walker, A. Tamai, A. de la Torre, T. Eknapakul, P. Buaphet, S.-K. Mo, W. Meevasana, M. S. Bahramy, and F. Baumberger, Nat. Commun. **5**, 3414 (2014).
[33] N. Bickel, G. Schmidt, K. Heinz, and K. Müller, Phys. Rev. Lett. **62**, 2009 (1989).
[34] M. E. Zvanut, S. Jeddy, E. Towett, G. M. Janowski, C. Brooks, and D. Schlom, J. Appl. Phys. **104**, 064122 (2008).
[35] Z. Hou and K. Terakura, J. Phys. Soc. Jpn. **79**, 114704 (2010).
[36] C. Lin and A. A. Demkov, Phys. Rev. Lett. **111**, 217601 (2013).